

UC Irvine

UC Irvine Previously Published Works

Title

Kinetic Analysis of Lipid Metabolism in Breast Cancer Cells via Nonlinear Optical Microscopy

Permalink

<https://escholarship.org/uc/item/91x4199j>

Journal

Biophysical Journal, 119(2)

ISSN

0006-3495

Authors

Hou, Jue

Reid, Nellone E

Tromberg, Bruce J

et al.

Publication Date

2020-07-01

DOI

10.1016/j.bpj.2020.06.007

Peer reviewed

Kinetic Analysis of Lipid Metabolism in Breast Cancer Cells via Nonlinear Optical Microscopy

Jue Hou,¹ Nellone E. Reid,² Bruce J. Tromberg,¹ and Eric O. Potma^{1,*}

¹Beckman Laser Institute and Medical Center, University of California, Irvine, Irvine, California and ²Department of Chemical and Materials Engineering, New Jersey Institute of Technology, Newark, New Jersey

ABSTRACT Investigating the behavior of breast cancer cells via reaction kinetics may help unravel the mechanisms that underlie metabolic changes in tumors. However, obtaining human in vivo kinetic data is challenging because of difficulties associated with measuring these parameters. Nondestructive methods of measuring lipid content in live cells provide a novel approach to quantitatively model lipid synthesis and consumption. In this study, coherent Raman scattering microscopy was used to probe de novo intracellular lipid content. Combining nonlinear optical microscopy and Michaelis-Menten kinetics-based simulations, we isolated fatty acid synthesis/consumption rates and elucidated effects of altered lipid metabolism in T47D breast cancer cells. When treated with 17 β -estradiol, the lipid utilization in cancer cells jumped by twofold. Meanwhile, the rate of de novo lipid synthesis in cancer cells treated with 17 β -estradiol was increased by 42%. To test the model in extreme metabolic conditions, we treated T47D cells with etomoxir. Our kinetic analysis demonstrated that the rate of key enzymatic reactions dropped by 75%. These results underline the capability to probe lipid alterations in live cells with minimum interruption and to characterize lipid metabolism in breast cancer cells via quantitative kinetic models and parameters.

SIGNIFICANCE Combining coherent Raman scattering microscopy and deuterium labeling provides insight into lipid metabolism in live cancer cells during cancer development and progression. The dynamic metabolic data are modeled with Michaelis-Menten kinetics to independently quantify the lipid synthesis and utilization in cancer cells. Changes in lipid levels are found to originate from de novo lipid synthesis using glucose as a source, lipid consumption from β -oxidation, and lipid consumption from cell proliferation, processes that can be separately analyzed with the Michaelis-Menten model. In this work, we isolate fatty acid synthesis and consumption rates and elucidated effects of altered lipid metabolism in T47D breast cancer cells in response to 17 β -estradiol stimulation and etomoxir treatment, dynamic processes that cannot be easily observed without the application of appropriate models.

INTRODUCTION

The abnormal production of metabolites for the synthesis of cellular building blocks and signaling molecules is an emerging hallmark of cancer (1). Cancer cells utilize the intermediate products of glycolysis to fuel the biosynthesis of amino acids, nucleotides, and fatty acids to

support fast cell proliferation. Different cancer cell lines exhibit varied glucose, and lipid metabolic signatures correlated with their metastatic potential and cell proliferation rate both in vitro and in vivo (2–4). Moreover, tumor metabolism has been shown to predict cancer cell response to chemotherapy in early stages (5). Thus, quantitative analysis of cancer cell metabolic kinetics is of great importance in characterizing cancer cell behavior and unraveling the role of cell metabolism in cancer progression and transformation.

Biochemically, cell metabolism is achieved through a series of reactions of varying complexities, catalyzed by proteins or catalytic RNAs. The Michaelis-Menten equation is often used to quantify enzyme-related metabolic behavior in normal and mutated cells:

$$v_0 = \frac{V_{max}[S]}{K_M + [S]}, \quad (1)$$

where V_{max} is the maximum rate achieved by the reaction, $[S]$ is the substrate concentration, and K_M is the Michaelis-Menten constant or substrate concentration at which the reaction rate is half of V_{max} . By combining fluorescence, isotope, and radio labeling with Michaelis-Menten kinetics, cell metabolic rates can be investigated quantitatively. In a clinical study, $[3H]$ -labeled androstenedione and Michaelis-Menten kinetics were utilized to evaluate the effect of CYP191A gene mutation on aromatase metabolism (6). Similarly, Michaelis-Menten parameters were employed to study intracellular hydrolysis for the detection of breast cancer by measuring intracellular fluorescein intensity changes (7). However, most of these traditional labeling methods relied on exogenous chemicals that may compromise the living biological system in unknown ways. Moreover, the requirement for complicated sample preparation and time-consuming data acquisition impede the possibility of dynamic studies with high spatial and temporal resolution.

Multimodal, nonlinear optical microscopy enables minimally interrupted evaluation of cell metabolism with high spatial and temporal resolution. Previously, two-photon excited fluorescent microscopy was used to monitor cell glucose metabolism over a range of oxygen consumption conditions relevant for cancer imaging (8). By studying the intracellular lipid droplets with both coherent Raman scattering (CRS) microscopy and spontaneous Raman spectroscopy, Yue et al. (9) reported increased cholesterol accumulation in prostate cancer cells that correlated with cancer aggressiveness. Recently, CRS was utilized with deuterium labeling to quantify lipid metabolism. Zhang et al. (10) studied cancer anabolism after epithelial-mesenchymal transition by tracking the deuterium and alkyne vibrational signal with CRS. These research findings underline the potential of utilizing nonlinear optical microscopy to quantify live-cell metabolism with high spatial and temporal resolution.

In this study, quantitative models were derived and used to describe alterations of the glucose metabolic pathways in the context of lipid production and consumption in breast cancer cells. We used CRS microscopy to determine metabolically driven changes to the cell's lipid content. For this purpose, deuterium labeling was utilized to investigate de novo lipid synthesis in cancer cells. We monitored fatty acid synthesis from deuterated glucose and subsequent

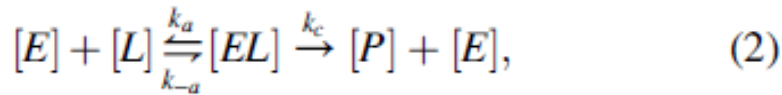
consumption by tracking the carbon-deuterium signal in a pulse-chase experiment. Recently, Zhang et al. (11) observed changes of glucose-supplied lipid renewal in sebaceous glands by combining CRS with deuterium labeling. However, the study was still based on observations of changes in the total lipid content and was thus unable to quantify lipid synthesis and consumption/degradation independently. Here, we combined CRS, deuterium labeling, and Michaelis-Menten kinetics modeling to isolate fatty acid synthesis and consumption rates. We revealed the effects of altered lipid metabolism in the estrogen-receptor-positive (ER β) T47D breast cancer cells when treated with 17 β -estradiol (E2). We also found that the T47D breast cancer cells exhibited elevated levels of lipid synthesis and utilization rates when activated by E2. Finally, we treated T47D breast cancer cells with etomoxir (ETO) to investigate the modeling efficiency in extreme β -oxidation inhibition conditions.

MATERIALS AND METHODS

Model development

Intracellular lipid homeostasis is a balance between lipid synthesis and consumption/degradation. Lipid synthesis is regulated by acetyl-CoA carboxylase, which is activated by citrate and inhibited by fatty acid palmitate (12). On the other hand, one of the most important pathways of lipid degradation (fatty acid oxidation) is regulated by mitochondria trifunctional protein. Both pathways have been observed to be dysregulated in many cancer cell lines to fuel the cancer proliferation and progression (13).

We first focus on lipid degradation. Assuming that the main enzymatic lipid degradation mechanism is β -oxidation, an enzymatically controlled process, we may start with the general form of substrate-enzyme interactions as described by Michaelis-Menten kinetics:



where $[E]$ is the enzyme concentration, $[L]$ is the lipid concentration, $[EL]$ is the enzyme-lipid complex, and $[P]$ is the oxidized lipid concentration. The change in lipid concentration is directly related to the formation of product:

$$\frac{d[L]}{dt} = -\frac{d[P]}{dt} = -k_c[EL]. \quad (3)$$

Next, we make the Michaelis-Menten approximation that the lipid is in chemical equilibrium with the complex, which means that

$$[EL] = \frac{k_a}{k_{-a}} [E][L] = K_a [E][L], \quad (4)$$

where $K_a = k_a/k_{-a}$ is the equilibrium constant for the formation of the lipid-enzyme complex. Applying the condition of conservation of the total enzyme concentration $[E_0]$,

$$[E_0] = [E] + [EL], \quad (5)$$

we find that the enzyme concentration can be written as follows:

$$[E] = \frac{[E_0]}{1 + K_a[L]}. \quad (6)$$

Using Eqs. 4 and 6 and substituting them in Eq. 3, we obtain the following:

$$\frac{d[L]}{dt} = -k_c K_a [E_0] \frac{[L]}{1 + K_a[L]} = -\frac{\alpha [L]}{1 + K_a[L]}, \quad (7)$$

where $\alpha = k_c K_a [E_0]$. In the experiment, the change in lipid is measured through the change in the fraction of deuterated lipids. Hence, the normalized lipid concentration measured in the experiment is $[L] [dLD]/[LD]$, where $[dLD]$ denotes the concentration of deuterated lipid in the lipid droplets of the breast cancer cells, and $[LD]$ is the concentration of nondeuterated lipids in the lipid droplets. Eq. 7 forms the starting point for our lipid degradation analysis. If needed, the model can be expanded to include uncompetitive substrate inhibition, in which the enzyme-lipid complex is inhibited through the adsorption of a second lipid substrate. In this case, the rate of change can be modeled as follows (14):

$$\frac{d[L]}{dt} = -\frac{\alpha [L]}{\delta + [L] + K_{L1}[L]^2}, \quad (8)$$

where $\delta = 1/K_a$ and K_{L1} is the equilibrium constant of the formation of the enzyme-lipid complex with a second lipid adsorbed.

The mechanisms that contribute to enzymatically controlled loss of lipids related to b-oxidation, captured by Eqs. 7 and 8, can be denoted by the rate $D_e([L])$. Besides the $D_e([L])$ mechanisms, the lipid pool can also be affected by nonenzymatic oxidation reactions (15). Accounting for first- and zero-order nonenzymatic degradation mechanisms, the change in lipid concentration can be written as follows:

$$\frac{d[L]}{dt} = D_e([L]) - k_1[L] - k_0 = D([L]), \quad (9)$$

where k_0 is the zero-order rate, and k_1 is the first-order nonenzymatic rate of lipid degradation. The total rate of lipid loss is summarized by $D(L)$. The different versions of the lipid degradation mechanism examined in this work are summarized in Table 1.

In this study, we considered lipid synthesis from deuterated glucose. Because δ -glucose is in excess, we may model the change in deuterated lipid concentration as a zero-order kinetic contribution as follows:

$$\frac{d[L]}{dt} = k_s - D([L]), \quad (10)$$

where k_s is the zero-order reaction rate for lipid synthesis. Here, the change in deuterated lipid concentration is thus a balance between lipid synthesis and lipid consumption/degradation. To describe the situation of lipid accumulation, Eq. 10 was used in conjunction with the lipid degradation models discussed in Table 1.

TABLE 1 Different Lipid Degradation Mechanisms Examined in This Work

Model	Rate Equation	Description of Degradation Mechanism
I	$\frac{d[L]}{dt} = - \frac{\alpha[L]}{1+K_a[L]}$	enzymatic
II	$\frac{d[L]}{dt} = - \frac{\alpha[L]}{1+K_a[L]} - k_0$	enzymatic with zero-order nonenzymatic degradation
III	$\frac{d[L]}{dt} = - \frac{\alpha[L]}{1+K_a[L]} - k_1 [L]$	enzymatic with first-order nonenzymatic degradation
IV	$\frac{d[L]}{dt} = - \frac{\alpha[L]}{\delta+[L]+K_{IJ}[L]^2}$	enzymatic with inhibition
V	$\frac{d[L]}{dt} = - \frac{\alpha[L]}{\delta+[L]+K_{IJ}[L]^2} - k_0$	enzymatic with inhibition plus zero-order nonenzymatic degradation
VI	$\frac{d[L]}{dt} = - \frac{\alpha[L]}{\delta+[L]+K_{IJ}[L]^2} - k_1 [L]$	enzymatic with inhibition plus first-order nonenzymatic degradation

Fitting procedure

Data from lipid synthesis and pulse-chase experiments were fitted to the models listed in Table 1, using a MATLAB (The MathWorks, Natick, MA) minimization routine. Using a numerical ordinary differential equation solver (ode45), the code fits the data by minimizing the sum of the square of the differences between the predicted and experiment data. The fminsearch function in MATLAB is used, and the iterative process continues until the algorithm has found the fitted parameters that minimize this difference. Accuracy of fitting was measured using the square of Pearson's correlation coefficient (r^2). The correlation coefficient indicates how well the calculated curve fits the original data, with a value ranging from zero to one. The closer the correlation coefficient is to 1.0, the better the fit. Models were eliminated if r^2 -values were low ($r^2 < 0.90$) or fitted parameters resulted in a negative value (not physically possible). In addition, confidence intervals were measured graphically to determine the significance of each parameter against experimental data using a 95% confidence interval. The code used for fitting is provided as Data S1.

To find the best description of the data, the simplest Michaelis-Menten model was examined first (i.e., model I, for the case of the pulse-chase experiments (lipid degradation)). If the fitting criteria were not met, the model was subsequently expanded with more parameters, as listed in Table 1. If further expansion did not improve the fit ($r^2 \geq 0.90$) any further over a simpler model with fewer fitting parameters, then the simpler model was retained.

Stimulated Raman scattering measurements

A 76-MHz Nd:Vanadate laser at 1064 nm (picoTrain; High Q, Rankweil, Austria) was used, producing a 7-ps pulsed laser beam (Stokes beam). The second harmonic of the same laser (532 nm) was used to pump an optical parametric oscillator (Levante Emerald; Applied Physics & Electronics, Fremont, CA) to provide the corresponding pump beam for imaging either the C-H lipid distribution (817 nm for a Raman shift of 2845 cm^{-1}) or C-D lipid signal (864 nm for a Raman shift of 2175 cm^{-1}). The Stokes beam was modulated with an acousto-optic modulator (12465; Crystal Technology, Westchester, PA) at 10 MHz. Both the Stokes beam and pump beam were spatially and temporally overlapped and delivered to a laser-scanning microscope (IX71; Olympus, Center Valley, PA). The maximum average power at the sample was 15 mW per beam. The CRS signal was detected in the forward direction. For this purpose, the pump beam was focused onto a photodiode (FDS1010; Thorlabs, Newton, NJ) with a high optical density (O.D.) bandpass filter for blocking the Stokes beam. The output of the photodiode was filtered with an electronic bandpass filter (BBP-10.7+; Mini-Circuits, Brooklyn, NY) and demodulated by a homemade lock-in amplifier to detect the Raman loss signal. The cells were imaged by a 60x water objective (1.2 NA, UPLANSAPO; Olympus), and the CRS signal was collected in the forward direction by a condenser (NA = 1.05). An olive oil sample was measured before each experiment for calibration purposes. Images were acquired as 512 x 512 pixel maps. The pixel dwell time was 4 μs for a total frame rate of 1 Hz. 10 frames were averaged to improve the signal/noise ratio.

Cell culture

The T47D breast cancer cell line was acquired from American Type Culture Collection (ATCC; Manassas, VA). The normal cell culture medium is made from Advance Dulbecco's Modified Eagle's Medium (DMEM)/F-12 culture medium (A2494301; Thermo Fisher Scientific, Waltham, MA) supplemented with 5% fetal bovine serum (12676011; Corning, Corning, NY), 1% GlutaMAX (35050-061; Life Technologies, Carlsbad, CA), 147.5 mg/L L-arginine (A5006; Sigma-Aldrich, St. Louis, MO), 91.25 mg/L L-lysine (L5501; Sigma-Aldrich), and 3151 mg/L normal glucose (G7021; Sigma-Aldrich). The deuterated medium was prepared by replacing the normal glucose with deuterated glucose (552003; Sigma-Aldrich) of the same concentration. The cells were cultured at 37°C and 5% CO₂. The cells were monitored daily, and the culture medium was changed every 2–3 days. For all the experiments, the cells were detached and collected at around 60% confluence with TrypLE (12604013; Life Technologies).

For lipid synthesis experiments, the cells were harvested and plated onto coverslips at 50,000 cells per well in 24-well plates. The cells were incubated in normal culture medium for 24 h to allow the cells to recover. The cells were then switched to serum-free culture medium

overnight for cell cycle synchronization. Subsequently, the cells were exposed to deuterated culture medium (considered $T = 0$). One plate of the cells was treated with 10^{-8} M E2 (E8875; Sigma-Aldrich), and the other plate of the cells was treated with dimethyl sulfoxide (DMSO) at the same concentration. We fixed two wells (two replicates) for each plate at $T = 0, 2, 3, 4, 5, 6,$ and 9 h in 4% formaldehyde.

For pulse-chase experiments, the cells were harvested and plated onto coverslips at 50,000 cells per well in 24-well plates. The cells were incubated in normal culture medium for 24 h to allow the cells to recover and switched to deuterated glucose medium for 24 h. To test the effect of E2, one plate of the cells was treated with 10^{-8} M E2 and the other plate of cells was treated with 10^{-8} M DMSO. To test the effect of ETO, one plate of the cells was treated with 4×10^{-5} M ETO, and the other plate of the cells was treated with 4×10^{-5} M vehicle control. The cells were then switched to normal glucose medium (considered $T = 0$), and two wells (replicates) of the control group and experimental group were fixed at times $T = 0, 2, 4, 6, 9,$ and 12 h.

Lipid quantification

The CRS images were imported into ImageJ. The image intensities were first calibrated by the olive oil reference sample as

$$I_{cal} = (I - I_{min}) \times \frac{I_{ref1}}{I_{ref}}, \quad (11)$$

where I_{cal} is the calibrated signal, I is the direct measured signal intensity, I_{min} is the minimum intensity in the image, I_{ref} is the mean intensity of the olive oil sample measured before the experiment, and I_{ref1} is the mean intensity of the olive oil reference sample measured repeatedly during the day. The purpose of the I_{ref1}/I_{ref} term is to correct for system performance variations during imaging sessions. The calibration was done only on 2845 cm^{-1} . The experiment was halted for system inspection if the difference between I_{ref} and I_{ref1} exceeded 10%.

In this work, we focus on lipid quantification by determining the changes in lipid content contained by intracellular lipid droplets. Lipid droplets are reservoirs for neutral lipids that can be easily identified in the cell. Because the droplets contain predominantly lipids and only limited amounts of protein, they form an ideal target for lipid quantification measurements. In each field of view, both the normal lipid distribution and deuterated lipid distribution were taken sequentially by tuning the wavelength of pump beam. All the images were first imported into MATLAB to calibrate their intensities and remove the background by five-component Otsu thresholding. The first component was considered background, and the average pixel intensity of the background pixels was calculated as I_{min} . Then, the processed images were analyzed in ImageJ, where 25 lipid droplets were randomly selected and manually outlined. The average C-H signal ($[LD]$) and deuterated signal ($[dLD]$) intensities within each lipid droplet were measured, and the lipid content was defined as the intensity ratios $[dLD]/[LD]$ for the same droplet. Because the deuterated fraction of lipids is small (i.e., $[dLD] \ll [LD]$), the C-H signal serves as a measure

of the total lipid content. This implies that the ratio $[dLD]/[LD]$ can be understood as the fraction of deuterated lipids relative to the total amount of lipid in the droplet.

RESULTS AND DISCUSSION

To validate the modeling approach, we measured the changes of the deuterated lipid signal in T47D breast cancer cells treated with either E2 or DMSO. We first cultured the cells in deuterated glucose medium for 24 h to label all intracellular lipid content with deuterium. Then, we switched all the cells to normal glucose culture medium and started to monitor the intensity changes of the coherent Raman signal that originated from the carbon-deuterium vibrational mode. The pulse-chase experiment lasted for 24 h, and the decay of deuterated lipid signal in T47D cells treated with either DMSO or E2 was recorded. T47D is an ER⁺ breast cancer cell line. As expected, ER⁺ breast cancer cells were sensitive to E2 treatment and responded with altered cell metabolism and proliferation. We used this experiment to test the sensitivity and accuracy of our simulation to clinically related cell metabolic changes. The raw data for fitting are summarized in Table S1.

Evaluating the efficiency of using different Michaelis-Menten model to simulate cancer metabolism

The data we collected during the pulse-chase experiment were fitted with all the kinetic models presented in Table 1. Note that the pulse-chase measurements represent the case of (deuterated) lipid degradation without synthesis, permitting a focus on degradation alone. The kinetic rate constants were obtained from nonlinear regression of the rate equations. The r^2 -values, kinetic rate constants, and concentrations were compared between all the models. All measurements were under at the same temperature to ensure the equilibrium constant K_a , which represents the affinity for the lipid and enzyme to form a complex, stays unchanged. In this context, we have assumed that K_a is a characteristic of lipid-enzyme association and that it remains unaltered under the conditions examined. The K_a was first determined with the E2 control experiment and kept constant within each model.

The simplest model that reproduces the experimental data with $r^2 > 0.90$ includes enzymatic lipid degradation in addition to first-order nonenzymatic degradation, as presented by model III. Note that without nonenzymatic degradation, the fitting criteria were not met, indicating that nonenzymatic lipid utilization mechanisms play a significant role. Including uncompetitive substrate inhibition or zero-order terms does not significantly improve the fit. In analyzing the following experiments, we used the simplest model (model III) to extract meaningful kinetic parameters from the data, the results of which are summarized in Table 2. Note that similar Michaelis-Menten parameter values were found for metabolite formation in other breast cancer studies (16).

TABLE 2 Kinetic Parameters of Lipid Synthesis and Enzymatic and Nonenzymatic Lipid Degradation

Model III Parameters	k_s	α	k_1	K_a
E2 control lipid degradation	–	0.208 ± 0.039	0.116 ± 0.013	72.72
E2-treated lipid degradation	–	0.404 ± 0.040	0.112 ± 0.009	72.72
E2 control lipid synthesis	0.026 ± 0.005	0.208	0.116	72.72
E2-treated lipid synthesis	0.037 ± 0.004	0.404	0.112	72.72
ETO control lipid degradation	–	0.290 ± 0.076	0.114 ± 0.021	72.72
ETO-treated lipid degradation	–	0.068 ± 0.096	0.290 ± 0.053	72.72

The indicated margins refer to the 95% confidence interval.

Kinetic model reveals the effect of E2 on an ER+ breast cancer cell line

Previously, an increased cell proliferation rate and cancer invasiveness were observed in T47D cancer cells upon treatment with E2 (17). The change of cancer cell phenotype has been known to alter cancer cell lipid consumption and lipid synthesis. To uncouple lipid synthesis from consumption, it is required to monitor both the deuterated lipid decay and deuterated lipid accumulation. Hence, we studied 1) the increase of the deuterated signal in normal T47D cells cultured in deuterated glucose medium and 2) the decrease of the deuterated signal in deuterated T47D cells cultured in normal glucose medium. The deuterated lipid signal decay was first fitted with model III to extract α and the nonenzymatic (k_1) lipid utilization rate. In addition, the equilibrium constant within model III was found as $K_a = 72.72$. The fitting procedure yields α and k_1 . Because $\alpha = k_c K_a [E_0]$, relative changes in $k_c [E_0]$ between experiments can thus be determined, which is a direct measure for the efficiency of enzymatic lipid degradation. For the fitting of lipid synthesis, the additional lipid synthesis rate k_s was determined using model III and Eq. 10.

The CRS images taken at 2175 cm^{-1} showed significant deuterated lipid deposition in cancer cells cultured with deuterated glucose after 24 h of culturing in deuterated medium (Fig. 1, a and b). After switching to the normal glucose culture medium, the deuterated lipid droplets signal intensity dropped to background levels within 12 h in cancer cells treated with E2 (Fig. 1 c). At $T = 9$ h, the signal intensity was six times higher in the cancer cells treated with DMSO. In the lipid synthesis study, the deuterated lipids became visible as early as 2 h in both conditions. Both cancer cells in the DMSO and E2-treated groups demonstrated a rapid increase in deuterated signal from 2 to 6 h (Fig. 1 d). After 9 h of culturing, the growth of the deuterated signal levels off for both conditions. However, the cells treated with E2 demonstrated 1.6 times

higher signal intensity over the control group after 9 h. Overall, the model reproduces both the lipid degradation and the lipid synthesis profiles with a consistent set of fitting parameters. Yet, the last data point at $T = 9$ is less well reproduced, and longer-term studies are required to verify the accuracy of the model at later times.

From the CRS images, the signal intensities in cancer cells treated with E2 demonstrated a higher decay rate, indicating increased lipid consumption/degradation. By fitting the data to the model, we found that the cells treated with E2 showed a 94% relative increase in k_d (Table 2), indicating an increase of lipid utilization. However, the nonenzymatic activities in both experimental conditions remained at a similar level. The latter implies that E2 treatment primarily affects the enzymatic degradation of lipid, such as β -oxidation, whereas the nonenzymatic lipid consumption is not directly affected by the treatment. In addition, analysis of lipid synthesis revealed that the cancer cells treated with E2 display increased de novo lipid synthesis along with enhanced lipid consumption. The E2-treated cancer cells had 42% higher k_s -values compared with the cells treated with DMSO. It is known that the E2 treatment can increase cancer cell proliferation. To meet the high demand for lipid during organelle and membrane replication, the cancer cells respond by increasing lipid synthesis, as confirmed by our simple kinetic analysis.

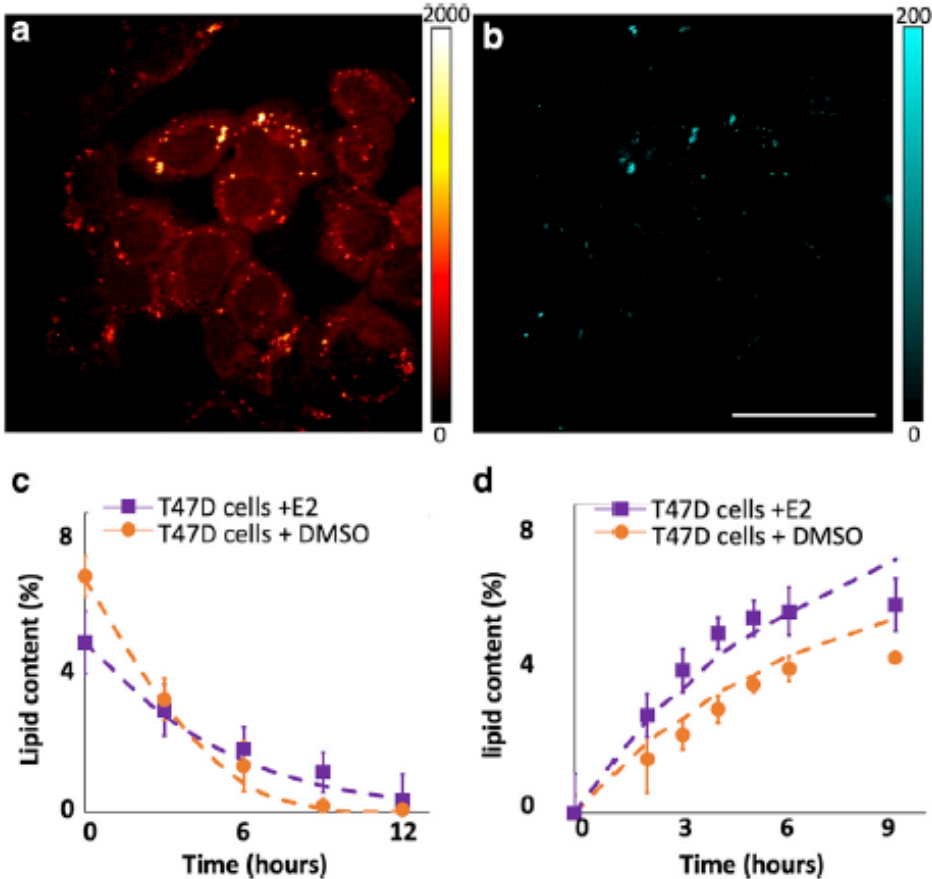


FIGURE 1 Deuterated lipid pulse-chase experiments of lipid synthesis and lipid consumption. Representative (a) normal lipid distribution (817 nm pump laser) and (b) corresponding deuterated lipid distribution (869 nm pump laser) in T47D cancer cells at $T = 0$ h. (c) Measured decay of normalized lipid content in T47D cells (control) and 17 β -estradiol (E2)-treated T47D cells fitted to model III. (d) Measured transient of lipid synthesis in T47D cells (control) and 17 E2-treated T47D cells fitted to model III with zero-order lipid synthesis. Error bars represent the SD from 25 randomly picked lipid droplets. Scale bars, 20 μ m. To see this figure in color, go online.

These observations retrieved from CRS imaging and kinetic modeling corroborate previous work. It has been re-reported that ER activation in ER⁺ cell lines can increase the cellular uptake of multiple types of fatty acid (18). In other independent studies, the activation of ER by estradiol has also been reported to upregulate the expression of trifunctional protein β -subunit (HADHB) and fatty acid elongation of very long-chain fatty acids 2 (ELOVL2) to increase β -oxidation (19,20). Thus, an increase of reaction substrate (fatty acid) and elevated enzyme activity contributed in concert to the rise of lipid utilization. The altered lipid metabolism provides energy and biomass support of cancer progression and proliferation. Rather than a qualitative description, our kinetic analysis provided a quantitative view of the intracellular bioreactions in living cells without labeling.

Sensitivity of the model to changes of lipid metabolism

To further test the utility of the kinetic model in extreme conditions, breast cancer cells were treated with ETO. ETO constrains cell β -oxidation by inhibiting carnitine palmitoyltransferase-1 (CPT1) on the outer mitochondrial membrane. Similar to the experiments discussed above, T47D breast cancer cells were first cultured in deuterated glucose for 24 h before switching to normal culture medium. The deuterated signal decay from the lipid droplets was measured over 12 h.

At time $T = 0$, the signal intensity was similar in both experimental groups. In the control group, the deuterium signal dropped to background levels after 9 h of culturing (Fig. 2, a and b). However, the deuterated lipid droplets were still visible in the T47D cells treated with ETO after 12 h and remained at a constant level (Fig. 2, c–e). ETO inhibits the CPT1 protein, which catalyzes the transfer of the acyl group of a long-chain fatty acid in the cytosol to enable its internalization into the intermembrane space of mitochondria (21). The CPT1 protein is upstream from the β -oxidation process and limits the amount of substrate that is available for the final reaction. In our analysis, the a -value of the ETO control group is comparable with the E2 control group, showing the stability of the imaging system and the robustness of the model. However, the ETO-treated group demonstrated a 75% drop of a -value, indicating a lack of lipid available for β -oxidation and a much lower lipid utilization rate. It is known that ETO treatment adversely affects normal metabolic pathways and cell viability (22). Thus, we observed a significant increase of the nonenzymatic lipid utilization (k_1) in the cells treated with ETO. The doubled nonenzymatic lipid utilization can be due to the loss of cell integrity during apoptosis. It further proved the necessity to include the first-order nonenzymatic lipid degradation term, which acts as an indicator of overall cell health. These kinetic findings generally confirm the altered lipid metabolism by ETO.

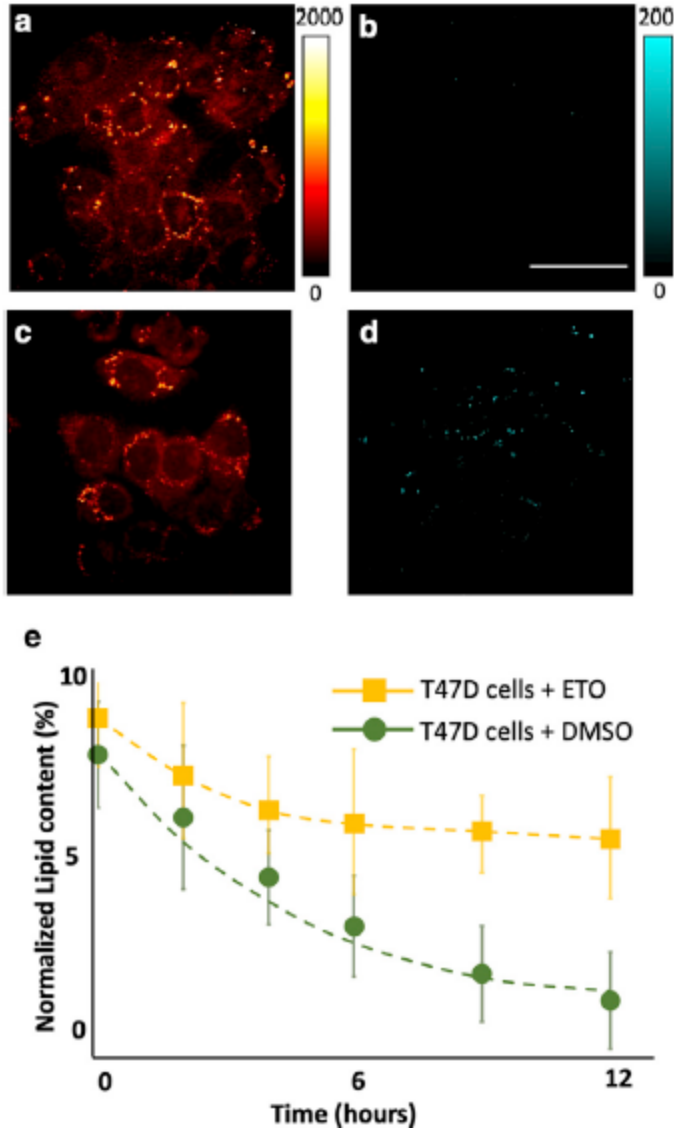


FIGURE 2 Pulse-chase experiments of ETO-treated T47D cancer cells. CRS images of representative normal lipid distribution at T = 12 h for (a) DMSO-treated T47D cells and (c) ETO-treated T47D cells. CRS images of representative deuterated lipid distribution at T = 12 h for (b) DMSO-treated T47D cells and (d) ETO-treated T47D cells. (e) Measured decay of normalized lipid content in T47D cells treated with either DMSO or ETO, fitted to a modified single substrate lipid consumption with cell proliferation kinetic model. The error bars represent the SD from 25 randomly picked lipid droplets. Scale bars, 20 μm . To see this figure in color, go on-line.

CONCLUSIONS

We have combined CRS imaging with quantitative kinetic modeling to reveal the effect of E2 on ER+ breast cancer cells. We observed that when treated with E2, cancer cells show an increase in the lipid utilization rate as well as de novo lipid synthesis. With Michaelis-Menten

modeling, we quantified the rate of substrate binding and the enzyme reaction rate in related pathways. We observed a synergetic increase of lipid supply and enzyme reaction rate to fuel the high lipid utilization rate of ER⁺ cancer cells activated by E2. At the same time, we observed increased lipid synthesis in E2-treated ER⁺ cancer cells. The cells utilize the intermediate product of glycolysis (citrate) for de novo lipid synthesis to fuel the high demand of biomass during cancer proliferation. Moreover, the binding of E2 to the estrogen receptor α (ER α) upregulates the expression of the glucose transporter and increases the influx of glucose molecules to support the biosynthesis. Our kinetic analysis also worked in otherwise extreme metabolic conditions. It predicted the effect of ETO on limiting the β -oxidation rate and decreasing lipid utilization. The nonenzymatic coefficient k_1 showed limited variation in the control groups and cells treated with E2. However, nonenzymatic lipid utilization almost doubled in the cells treated with ETO as a result of reduced cell viability. Taken together, our observations match with previously published work and underline the utility of combining CRS and Michaelis-Menten modeling to quantify live-cell metabolism with minimum interruption.

SUPPORTING MATERIAL

Supporting Material can be found online at <https://doi.org/10.1016/j.bpj.2020.06.007>.

AUTHOR CONTRIBUTIONS

J.H. designed research, performed research, analyzed data, and wrote the manuscript. N.E.R. designed research, performed research, developed kinetic models, analyzed kinetic models with respect to data, and wrote the manuscript. B.J.T. designed research and wrote the manuscript. E.O.P. de-signed research and wrote the manuscript.

ACKNOWLEDGMENTS

This work was supported by National Institute of Biomedical Imaging and Bioengineering (P41EB015890), National Cancer Institute (R01CA142989 and R01CA195466), National Institute of General Medical Sciences (R01GM132506), the National Cancer Institute Chao Family Comprehensive Cancer Center (P30CA62203), the University of California Historically Black Colleges and Universities Initiative, and the Arnold and Mabel Beckman Foundation.

REFERENCES

1. Hanahan, D., and R. A. Weinberg. 2011. Hallmarks of cancer: the next generation. *Cell*. 144:646–674.
2. Li, Z., and Y. Kang. 2017. Lipid metabolism fuels cancer's spread. *Cell Metab.* 25:228–230.
3. Weng, M.-S., C.-T. Ho, ., J.-K. Lin. 2007. Theanaphthoquinone inhibits fatty acid synthase expression in EGF-stimulated human breast cancer cells via the regulation of EGFR/ErbB-2 signaling. *Toxicol. Appl. Pharmacol.* 218:107–118.

4. Hou, J., J. Williams, ., B. J. Tromberg. 2018. Visualization of breast cancer metabolism using multimodal nonlinear optical microscopy of cellular lipids and redox state. *Cancer Res.* 78:2503–2512.
5. Walsh, A. J., R. S. Cook, and M. C. Skala. 2017. Functional optical imaging of primary human tumor organoids: development of a personalized drug screen. *J. Nucl. Med.* 58:1367–1372.
6. Chen, Z., O. Wang, ., X. Xing. 2015. Aromatase deficiency in a Chinese adult man caused by novel compound heterozygous CYP19A1 mutations: effects of estrogen replacement therapy on the bone, lipid, liver and glucose metabolism. *Mol. Cell. Endocrinol.* 399:32–42.
7. Blokh, D., I. Stambler, ., M. Deutsch. 2007. The information-theory analysis of Michaelis-Menten constants for detection of breast cancer. *Cancer Detect. Prev.* 31:489–498.
8. Hou, J., H. J. Wright, ., B. J. Tromberg. 2016. Correlating two-photon excited fluorescence imaging of breast cancer cellular redox state with Seahorse flux analysis of normalized cellular oxygen consumption. *J. Biomed. Opt.* 21:60503.
9. Yue, S., J. Li, ., J.-X. Cheng. 2014. Cholesteryl ester accumulation induced by PTEN loss and PI3K/AKT activation underlies human prostate cancer aggressiveness. *Cell Metab.* 19:393–406.
10. Zhang, L., and W. Min. 2017. Bioorthogonal chemical imaging of metabolic changes during epithelial-mesenchymal transition of cancer cells by stimulated Raman scattering microscopy. *J. Biomed. Opt.* 22:1–7.
11. Zhang, L., L. Shi, ., W. Min. 2019. Spectral tracing of deuterium for imaging glucose metabolism. *Nat. Biomed. Eng.* 3:402–413.
12. Chajès, V., M. Cambot, ., V. Joulin. 2006. Acetyl-coA carboxylase alpha is essential to breast cancer cell survival. *Cancer Res.* 66:5287–5294.
13. Zaugg, K., Y. Yao, ., T. W. Mak. 2011. Carnitine palmitoyltransferase 1C promotes cell survival and tumor growth under conditions of metabolic stress. *Genes Dev.* 25:1041–1051.
14. Leow, J. W. H., and E. C. Y. Chan. 2019. Atypical Michaelis-Menten kinetics in cytochrome P450 enzymes: a focus on substrate inhibition. *Biochem. Pharmacol.* 169:113615.
15. Walther, T. C., and R. V. Farese, Jr. 2012. Lipid droplets and cellular lipid metabolism. *Annu. Rev. Biochem.* 81:687–714.
16. Zhou, X., S. Wang, ., B. Wu. 2015. Sulfonation of raloxifene in HEK293 cells overexpressing SULT1A3: involvement of breast cancer resistance protein (BCRP/ABCG2) and multidrug resistance-associated protein 4 (MRP4/ABCC4) in excretion of sulfate metabolites. *Drug Metab. Pharmacokinet.* 30:425–433.
17. Samavat, H., and M. S. Kurzer. 2015. Estrogen metabolism and breast cancer. *Cancer Lett.* 356:231–243.
18. Belkaid, A., R. J. Ouellette, and M. E. Surette. 2017. 17 β -estradiol-induced ACSL4 protein expression promotes an invasive phenotype in estrogen receptor positive mammary carcinoma cells. *Carcinogenesis.* 38:402–410.

19. Zhou, Z., J. Zhou, and Y. Du. 2012. Estrogen receptor alpha interacts with mitochondrial protein HADHB and affects beta-oxidation activity. *Mol. Cell. Proteomics*. 11:M111.011056.
20. González-Bengtsson, A., A. Asadi, ., A. Jacobsson. 2016. Estrogen enhances the expression of the polyunsaturated fatty acid elongase Elov12 via ER α in breast cancer cells. *PLoS One*. 11:e0164241.
21. Kruszynska, Y. T., and H. S. Sherratt. 1987. Glucose kinetics during acute and chronic treatment of rats with 2[6(4-chloro-phenoxy)hexyl] oxirane-2-carboxylate, etomoxir. *Biochem. Pharmacol.* 36:3917–3921.
22. Pike, L. S., A. L. Smift, ., M. Wu. 2011. Inhibition of fatty acid oxidation by etomoxir impairs NADPH production and increases reactive oxygen species resulting in ATP depletion and cell death in human glioblastoma cells. *Biochim. Biophys. Acta.* 1807:726–734.

*Correspondence: epotma@uci.edu

Jue Hou and Nellone E. Reid contributed equally to this work. Editor: Amy Palmer.